진동하는 조종면의 충격파 교란이 천음속 플러터 특성에 미치는 영향에 대한 연구

A Study on the Effect of Shock Interference of Oscillating Control Surface on Transonic Flutter Caracteristics

권혁준*, 유재한, 김종윤, 이인, 한재흥(KAIST), 김동현(경상대학교)

1. Introduction

Under flight conditions, the reduction of rotational stiffness on a flap hinge may occur because the actuator systems have failed or because the actual hinge stiffness is somewhat different from the designed hinge stiffness. Therefore, the observations of the effects of hinge stiffness reduction on flutter stability are necessary. In particular, if the shock waves are correlated with control surface motion in transonic regime, flutter becomes more dangerous.

In this paper, we introduce aeroelastic analysis results of a wing with an oscillating control surface and describe the various effects of rotational stiffness on the flutter characteristics. The aeroelastic analysis for the control surface model is so time-consuming that an effective three-dimensional aerodynamic theory is applied to investigate the aeroelastic characteristics in transonic and supersonic regimes. The unsteady aerodynamic code based on the modified transonic unsteady small disturbance (TSD) theory can be used to effectively analyze the unsteady aerodynamics of the aircraft wings with control surface

2. Theoretical Back Grounds

In the present study, aeroelastic analyses are performed in both the time and the frequency domain, and the computation results are compared with each other. The aeroelastic equation of motion can be formulated by Hamilton's Theorem for elastic models and is written in matrix form as follows:

$$[M_g]\{\ddot{q}(t)\}+[C_g]\{\dot{q}(t)\}+[K_g]\{q(t)\}=\{Q(t)\} \quad (1)$$

where, $\{q(t)\}$ is the generalized displacement vector and $[M_g]$, $[C_g]$, and $[K_g]$ express the generalized mass, damping, and stiffness matrices respectively. $\{Q(t)\}$ represent the generalized aerodynamic force as follows:

$$Q_i(t)=\tfrac{1}{2}\rho U^2 c_r^2 \int_s h_i(x,y)\Delta C_p(x,y,t)\, dS/c_r^2 \quad (2)$$

In this equation, subscript 'i' indicates the influence mode; S is the plane area of wing; and c_r, ρ, and U represent the root chord length, free stream density, and free stream velocity, respectively. In equations (1) and (2), symbol 't' represents physical time, so we must pay attention to the transition from non-dimensional time in the CFD code into physical time in the structural equation of motion. The generalized damping matrix $[C_g]$ is proportional damping.

To perform a time domain flutter analysis, the state vector form of equation (1) is introduced and can be written as

$$\{\dot{x}(t)\}=[A]\{x(t)\}+[B]\{u(t)\} \quad (3)$$

For nonlinear structural systems, a typical numerical technique such as the Runge-Kutta method can be commonly used. The details for the coupled time integrated method (CTIM) were described in Ref. 1-3.

In the frequency domain flutter analysis, a transient pulse method (TPM) was applied to calculate the generalized aerodynamic forces (GAFs), which are usually needed in frequency domain flutter analyses using p-k or V-g methods.

The generalized aerodynamic influence coefficient (GAIC) matrix is defined as follows:

$$Y_{ij} = \frac{FFT\{Q_{ij}(t)\}}{FFT\{q_j(t)\}} \tag{4}$$

where $FFT\{\}$ is the fast Fourier transformation. Q_{ij} and $q_j(t)$ are defined respectively as follows:

$$Q_{ij} = \iint_s \frac{h_i}{c_r} \Delta Cp_j(x,y,z,t) \frac{ds}{S} \tag{5}$$

$$q_j(t) = q_{0j} \exp\{-(\tau - 17.5\Delta\tau)^2 / 4\} \tag{6}$$

where Q_{ij} is the GAF matrix in the time domain, h_i is the ith mode shape vector, c_r is the root chord length of the wing, and ΔCp_j is the unsteady pressure distributions on the wing surface induced by the jth transient pulse displacement motion. S is the area of the wing plane form and ds is each grid-cell area on the wing surface. In equation (6), q_{0j} is the transient pulse magnification factor, which is usually set to between 0.001 and 0.01% of the amplitude of a nondimensionalized mode. The results indicate that Y_{ij} is the generalized influence coefficient (GAIC) matrix that is induced by mode j acting through the displacements of mode i. More information for frequency domain flutter analysis was described in Ref. 4.

3. Results and Discussion

In this study, wing models having oscillating control surfaces are investigated. The various rotational stiffness values are applied to the hinge of the control surface, and for each case we would investigate the changes in aeroelastic characteristics resulting from the oscillating control surfaces. The geometric configuration is presented in Fig.1. This model has a 31.9° sweep back angle at the leading edge, the taper ratio is 0.31, and the aspect ratio is 2.98. The wing section has the shape of the 64A004.8 airfoil.

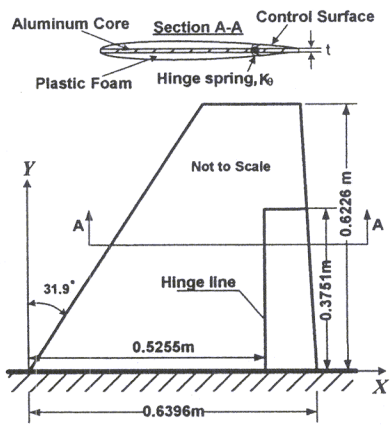

Fig. 1. Geometric configuration of wing model with flaperon.

	Mode 1	Mode 2	Mode 3
Clean Model	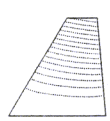	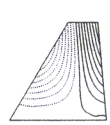	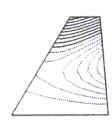
	8.76 Hz	33.96 Hz	45.80 Hz
HRS Model	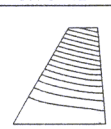	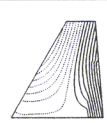	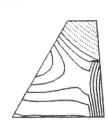
	8.31 Hz	28.83 Hz	37.52 Hz
LRS Model	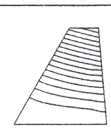	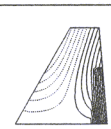	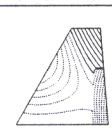
	8.31 Hz	27.37 Hz	35.39 Hz

Fig. 2. Comparisons of natural mode shapes and frequencies.

The free vibration analyses are accomplished by MSC/NASTRAN (Ver. 70.5). The natural mode shapes and frequencies of the first three modes are presented in Fig. 2. These free vibration analyses show that the first mode is simple bending but the higher modes include flap deflection. In this study, the first six modes were used in the aeroelastic analyses.

In the present study, the V-g method is applied to perform the frequency domain flutter analysis. The pulse method is used for the computation of the generalized aerodynamic influence coefficient matrix.

To examine the effects of the oscillating control surface, four different models are used, viz. a clean wing (CL) model, a low rotational stiffness (LRS) model, a high rotational stiffness (HRS) model, and a no flap oscillating effects (NFO) model. In the clean wing model, the wing has no control surface. The low rotational stiffness and high rotational stiffness models are classified according to the ratio of the flap rotational frequency to the reference frequency, $\omega_\beta / \omega_\alpha$. Here, $\omega_\beta = \sqrt{k_\theta / I_\alpha}$ and ω_α is the reference frequency. The second modal frequency is used for the reference frequency, ω_α, because the second mode is the first torsion mode. In the LRS model, $\omega_\beta / \omega_\alpha$ is 1.72 but in the HRS model, $\omega_\beta / \omega_\alpha$ is 2.77.

The calculated flutter speed and frequency boundaries of the clean wing model are shown in Fig. 3. In the subsonic region, the results of the coupled time integrated method (CTIM) are compared with that of the transient pulse method (TPM) and DLM. Because the airfoil thickness effect is not considered in the DLM, these results are additionally compared with the TPM results of the flat plate model and show good agreement. However, in the transonic regimes, there are some discrepancies because the shock interference severely affects the aeroelastic motion. The V-g and V-f plots for DLM and TPM results are shown in Fig. 4.

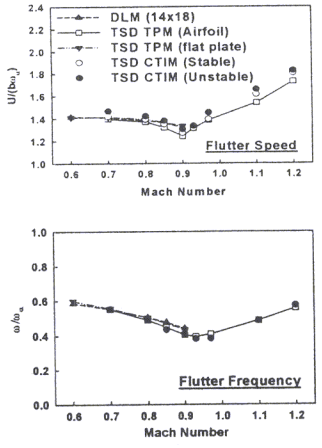

Fig. 3. Flutter boundary comparisons for clean wing model.

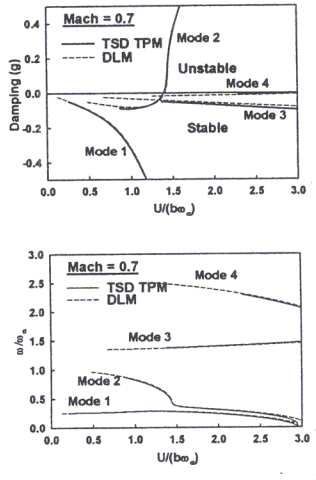

Fig. 4. V-g and V-f plots for clean wing model.

The aeroelastic analyses are performed for the low and high rotational stiffness models ($\omega_\beta / \omega_\alpha$ =1.72 and $\omega_\beta / \omega_\alpha$ =2.77). Figure 5 shows the flutter responses at Mach 1.1. When $\omega_\beta / \omega_\alpha$ is 1.72 (LRS model), the response of the flap shows a simple harmonic motion. This means that the third mode is dominant in the unstable response. For the high rotational stiffness (HRS) model, however, the fourth mode participates in the unstable motion and the phase plot

represents the multi-periodic pattern. Figure 6 shows the spectral density function of the physical responses at Mach 1.1. In Fig. 6a, the spectrums of the responses of the LRS model are similar to that of a simple harmonic response with the normalized frequency of 1.39. However, when the rotational stiffness is increased, the auto-spectral density plot shows that the response has two modal frequencies and, then, the lower mode of them disappears as shown in Fig 6b. Therefore, the auto-spectral density function represents the simple harmonic motion with a normalized frequency of 2.01. At Mach 1.1, in the LRS model, the second and third modes are unstable modes, however in HRS model, only the fourth mode is unstable.

Figure 7 shows the flutter boundary of the LRS and the HRS models. It also contains the comparison of the no flap oscillating effects (NFO) model. In this figure, "NFO" indicates that the unsteady aerodynamic effects of the local rotation of flap are ignored. In Fig 7a, when the oscillating effects are considered, the large decrease of flutter speed appears near Mach 1.0. Moreover, unlike the NFO models, the flap oscillating models have higher flutter frequencies than the third modal frequency. Therefore, we can find that nonlinear aerodynamic effects such as shock interference can cause severe decreases in flutter speed. Also, these phenomena are closely related to the transition of the dominant flutter mode with higher natural frequencies. The effects of the uncoupled frequency ratio, $\omega_\beta / \omega_\alpha$, is also presented in Fig. 7. The rise of the flutter speed following Mach number is delayed in low supersonic regime when the flap rotational stiffness has decreased. Therefore, the flutter dip of LRS model is extended to higher Mach numbers than was the case with the HRS model. Figure 7 also shows that the large increments of flutter speed can be accompanied by the transition of the flutter mode to higher modes. This trend can be observed at Mach 1.1.

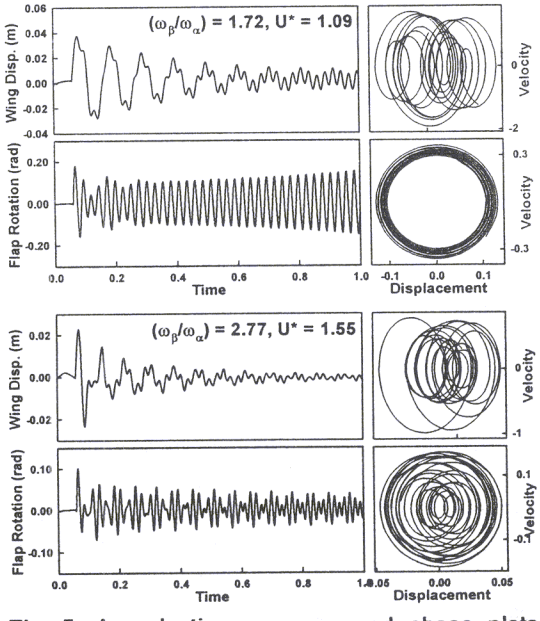

Fig. 5. Aeroelastic responses and phase plots of wing model with control surface at M=1.1.

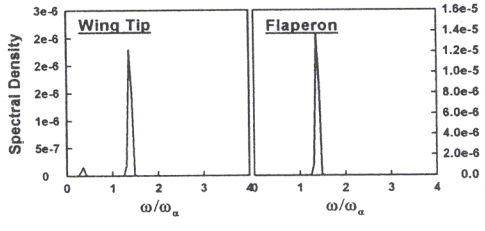

(a) $\omega_\beta / \omega_\alpha$ = 1.72 and U^* = 1.09

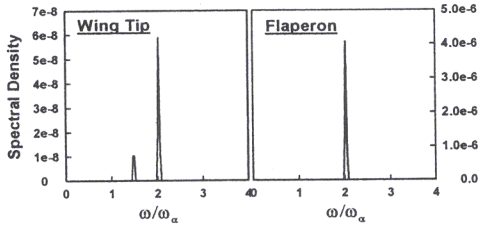

(b) $\omega_\beta / \omega_\alpha$ = 2.77 and U^* = 1.55

Fig. 6. Auto spectral density plots for wing and flaperon responses at M=1.1

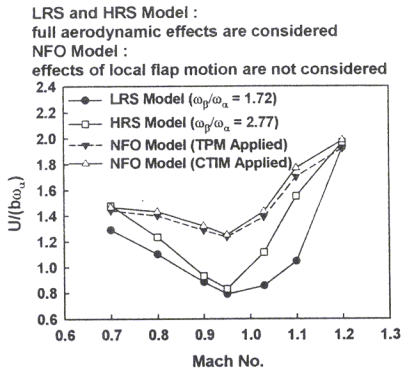

(a) Flutter speed

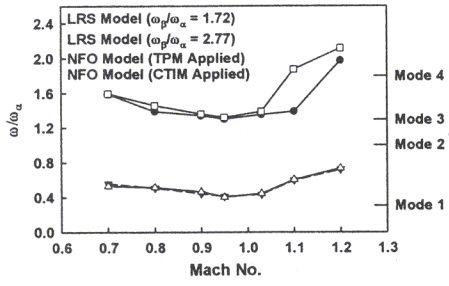

(b) Flutter frequency

Fig. 7. Comparisons of computed flutter characteristics for different rotational stiffness models

4. Conclusions

In this study, the transonic and supersonic flutter characteristics of wings with oscillating control surfaces were investigated using the frequency and time domain analysis scheme. In the frequency domain analysis, TPM and DLM were applied to calculate the generalized aerodynamic influence coefficients and the V-g method was used to determine the aeroelastic stability. The time domain flutter analyses were performed using a coupled time integration method (CTIM). The aeroelastic characteristics of the control surface models were compared to those of the NFO model to investigatethe unsteady aerodynamic effects of flap oscillation. These results showed that the unsteady aerodynamic interference cause severe decrease of the flutter speed. To examine the effects of rotational stiffness, aeroelastic analyses were performed for two different rotationalstiffness models. In addition, the large change on the flutter boundary was induced when the dominant mode on unstable motion was altered to another mode and the predicted dominant mode usually contained the flap motion.

Acknowledgements

This work was supported through funding from the Korea Ministry of Science and Technology. The authors acknowledge the support as the National Research Laboratory Program.

References

[1] Kim, D. H., Lee, I., "Transonic and Supersonic Flutter Characteristics of a Wing-Box Model with Tip Stores," 42nd AIAA/ASME/ASCE/AHS/ASC Structures, Structural Dynamics, and Materials Conf. & Exhibit 16-19 April 2001 at Seattle, AIAA Paper 2001-1464.

[2] Kim, D. H., Park, Y. M., Lee, I., Kwon, O. J., "Nonlinear Aeroelastic Computation of a Wing with a Finned-Store Using a Parallel Unstructured Euler Solver," 43rd AIAA/ASME/ASCE/AHS/ASC Structures, Structural Dynamics, and Materials Conf. & Exhibit, 22-25 April 2002 at Denver, AIAA Paper 2002-1289.

[3] 김동현, 권혁준, 이 인, "3차원 날개의 플러터 해석 결과와 풍동시험 결과의 비교연구", 한국항공우주학회지, 제28권, 제3호, 2000, pp. 53-63.

[4] Kim, D. H., Lee, I., "CFD-based matched-point transonic and supersonic flutter computations using a modified TSD equation," Computational Fluid Dynamics Journal 11-1, pp 44-54, 2002.